Journal of Neonatal Surgery
ISSN(Online): 2226-0439
Vol. 14, Issue 14s (2025)
https://www.jneonatalsurg.com

OPEN ACCESS

Segmentation of tumorous and non-tumorous using Contour Angular Section and Fuzzy C Means optimization

[1*] Dr.A.R.Deepa, [2] Dr.C.Thinkal Dayana, [3] Dr.Raju Shanmugam, [4] Dr.Vithya Ganesan , [5] Dr.C.Jaspin Jeba Sheela, [6] Dr.T.Vengatesh.

[1*] Associate Professor, Department of Computer Science and Engineering, Koneru Lakshmiah Education Foundation, Vaddeswaram, Guntur District, AP, India

Email ID: deepaamuth@gmail.com

[2] Assistant Professor, Scott Christian College (Autonomous), Nagercoil, Tamilnadu, India.

Email ID: thinkaldayana@gmail.com

[3] Dean – Academics, Professor, School of Computing, Vel Tech Rangarajan Dr.Sagunthala R&D Institute of Science and Technology

Email ID : srajuhere@gmail.com

[4] Professor, Department of CSE, Koneru Lakshmaiah Education Foundation, Vaddeswaram, AP, India

Email ID : vithyamtech@gmail.com

[5]Assistant Professor, Department of PG Computer Science, Nesamony Memorial Christian College, Marthandam, Tamilnadu, India.

Email ID : jaspinjebasheela@gmail.com

[6]Assistant Professor, Department of Computer Science, Government Arts and Science College, Veerapandi, Theni, Tamilnadu, India

Email ID: venkibiotinix@gmail.com

***Corresponding Author**

Dr.A.R.Deepa

Associate Professor, Department of Computer Science and Engineering, Koneru Lakshmiah Education Foundation, Vaddeswaram, Guntur District, AP, India

Email ID: deepaamuth@gmail.com

Cite this paper as: Dr.A.R.Deepa, Dr.C.Thinkal Dayana, Dr.Raju Shanmugam, Dr.Vithya Ganesan , Dr.C.Jaspin Jeba Sheela, Dr.T.Vengatesh (2025) Segmentation of tumorous and non-tumorous using Contour Angular Section and Fuzzy C Means optimization. *Journal of Neonatal Surgery*, 14 (14s), 1-24.

ABSTRACT

The brain is an vital part of the human body and helps to regulate all of a person's actions. It involves a huge number of activities such as thinking, reactions, feelings, memories, etc. Any brain disorder can have an impact on all aspects of human function. Tumors, strokes, and infections are examples of major brain diseases. If a brain tumour is not treated at an early stage, it is one of the deadliest illnesses. In this study, contour angular sections and FCM (Fuzzy C-Means) optimization were proposed as a precise method for segmenting MRI (Magnetic Resonance Image) brain tumours. With the use of a common MRI imaging technique, the tumour and non-tumor areas may be distinguished with ease. First-stage morphological reconstruction employs erosion, whereas second-stage morphological reconstruction employs dilation. An area is chosen for FCM optimization utilising the radius contraction and expansion method after the background reduction.

RCE (Radius Contraction and Expansion) provides the first selection of the region's and centroid's maximum radii by eliminating background noise. In magnetic resonance imaging(MRI), the contour angular sectioning (CAS) approach is employed to determine the RCE of tumours. It is challenging to segment brain tumours, hence the CAS optimization approach is recommended. The CAS optimization approach is encouraged for the difficult assignment of segmenting brain tumours. The contour is greater than the tumour region however almost the equal size as the tumor's region. A new estimate is made of the new contour's centroid region, which acts as one of the angular region's vertices. The contour's size is larger than the tumour region's size but around the same size as the tumor's shape. The new angular region that is eliminated clockwise is applied to FCM once again. This procedure is repeated until the development of an angular region, at which point one cycle of FCM optimization is complete. The usefulness of contour angular part and the utilization of MRI brain

tumour segmentation was once formerly evaluated via the use of the T1-weighted distinction in large image datasets, the usage of matrices like Dice Score (DS), Sensitivity, Specificity, Harsdorf Distance (HD), and probabilistic Rand Index (PRI). . The experimental outcomes exhibit that the contour angular part strategy works better than the most superior MRI brain tumour segmentation technique.

Keywords: *Contour, Brain tumor, Erosion, Dilation, Magnetic Resonance Image, optimization*

1. INTRODUCTION

The brain is often considered as the body's most state-of-the-art organ. A brain tumour is a grouping of extraordinary cells interior the brain that have grown in size or variety. Brain tumours may represent a serious threat. It is possible for this brain tumour to be benign, which means it does not cause cancer, or malignant, which does cause cancer. A benign tumour in the brain is a growth that develops slowly and is made up of cells that are not malignant. A malignant brain tumour, sometimes referred to as a cancerous brain tumour, is one that develops rapidly and has the potential to metastasize to the spine and other regions of the brain. For a huge vary of scientific analytical applications, the segmentation and localization of brain tumours from MR images are difficult and vital issues that should be resolved. The process of "segmenting" a brain tumour involves separating the cancerous growth from the surrounding healthy tissue in the brain. MRI and CT scans are two imaging modalities that may be used to investigate the anatomical structure of the human brain. An MRI imaging scan is used at several points during the procedure. MRI scans are now the most comfortable diagnostic examinations that can be performed. Because there is no radiation present, it will not have any impact on the human body in any way. Both the magnetic field and the radio waves are concentrated at its core.

One method for segmenting images is known as convolutional neural networks (CNNs). Three real datasets that depict various features of tumour development, such as location, dimensions, picture intensities, and enhancement, have been subjected to the image segmentation [1] technique (improvement). A method for segmenting images that combines the FCM algorithm and the K-means clustering method [2]. The most original technique for image segmentation, FCM clustering is also the smoothest and most effective. To accurately identify brain tumors, thresholding, which modifies an image's pixels to make them simpler to understand, is followed by level-set segmentation steps. The accuracy, processing speed, and performance of the partitioning technique known as image segmentation were assessed by contrasting them with various cutting-edge segmentation algorithms. The accuracy was determined by comparing the quality or state outcomes of each processed image to the original, raw data. The experimental findings of our algorithm have shown increased segmentation effectiveness by increasing segment quality and accuracy in a shorter amount of execution time. (Fully convolutional neural networks) FCNNs and (conditional random fields) CRFs have been earlier combined into a single framework to assemble a deep learning model for brain tumour segmentation [3]. In order to diagnose cancer, plan for therapy, and assess the effectiveness of that therapy, brain tumour segmentation must be accurate and trustworthy. Deep learning models that combine more than two segmentations consist of FCNNs, CRFs, multi-layer perceptron-based post-processing approaches, fully convolutional networks by using enhancing U-Net architecture, fluid vector flow (FVF), principal component analysis (PCA)[4], and support vector machines (SVM) [5].

Both generative and discriminative methodologies are now available for use in the segmentation of brain tumors. Since generative techniques explicitly characterise the chance distributions of anatomical aspects and the textural appearances of healthy tissues and tumours, they often exhibit right generalisation to images that have no longer until now been examined. This is performed by incorporating domain-specific prior expertise into the modelling system. On the other hand, creating correct models of the probabilistic distributions of brain tumours is a tough challenge. Discriminative techniques, on the other hand, work with the aid of first extracting facets from images and then associating these aspects with quite a number of tissue classifications through the use of discriminative classifiers. They frequently refer to supervised learning environments where the training approach is heavily dependent on images and voxel-wise class labels. Decision trees [6] and support vector machines are two examples of traditional approaches that fall within this category [7]. The novelty of our CAS-FCM-based segmentation for tumorous and non-tumorous brain MRI is that we can detect the tumorous MRI by segmentation. A contour angular section is used to maximise the readability of images. An MRI, which stands for magnetic resonance imaging, is a kind of examination that may be performed to locate a tumour in the body as well as to assist in determining whether or not a tumour is malignant. MRI scans are superior to CT scans in the detection of some malignancies, including cancers of the prostate and uterus as well as certain liver tumours. However, there were 77 MRIs that gave a false-negative result. A combined total of 51 malignancies were missed, while 26 were misread as something else. The parameters of an MRI, the kind of receptor, and the number of times malignancies were missed were shown to have no connection with one another. The accuracy of conventional MRI in identifying intracranial cancers is typically excellent; nevertheless, excessive reliance on this method should be avoided, particularly in the case of specific kinds of tumours. In instances where there is a disagreement, neurosurgeons are strongly urged to consult with the neuroradiologists who reported the findings in

order to arrive at the most accurate preoperative diagnosis. An MRI with contrast is essential in order to determine whether or not the therapy being administered to the patient who has a tumour is being carried out correctly. In most cases, MRI without contrast cannot be of use when attempting to evaluate the state of the tumour. Images obtained from an MRI with contrast are much easier to make out than those obtained from an MRI without contrast. Because of this, a contour angular section was used in order to improve the readability of the cancer on the MRI. As well as MRI image segmentation, which is the process of extracting known anatomic features from MRI scans and organising them into distinct regions, CAS-Fuzzy C-means, often known as FCM, is a clustering method that permits one piece of information to belong to two or more groups simultaneously. This is carried out through a parameterization device that is based totally on angles from the signature edge (2-D-shape), and it is used for off-line signature identification. The fuzzy set theory underpins fuzzy logic, which is a multi-valued logic. In addition to this, CAS-FCM has the potential to provide results that are superior to those produced by other clustering algorithms such as KM(K-Means), EM(Expectation Maximization), and KNN(K-Nearest Neighbors).

The following section contains a few publications that are linked to the various brain tumour segmentation investigations that are currently being conducted.

2. RELATED WORKS

In this part, the attempts that have been made to develop an automated approach for segmenting brain tumours are presented. [8],[9] refer to Deep Learning, K-Means Clustering, Concatenated Random Forests for Supervised, and Fully and Deep CNNs, respectively. Along with the Gaussian Mixture Model [10][11], Support Vector Machine (SVM) [12][13], and Fuzzy C-Means Algorithms [14], researchers have used a variety of techniques to slice brain tumours[15][16]. Using deep learning algorithms, enormous quantities of MRI-based picture recordings may be effectively processed and analyzed in an objective manner. This is possible because of these tactics. It places an emphasis on the deep learning methodologies that are now fashionable in this sector. First, a brief summary of brain tumours and the various approaches used to segment them is presented. The most recent advancements that have been made in deep learning tactics are brought to light before the most recent algorithms are analyzed. In the conclusion, a situational evaluation is provided, and prospective future tendencies to contain MRI-based brain tumour segmentation strategies into frequent clinical practise are recommended. Additionally, a novel Woelfel filter [17] may additionally be utilised to realize and section brain tumours. It combines anisotropic diffusion segmentation with augmentation and segmentation using morphological techniques. It is going to be determined where exactly the brain tumour is located. Convolutional neural networks (CNN) [18] are recommended as a method for improving accuracy in the modern world. It was trained using the BR35H benchmark dataset, which contains MRI images of brain tumours, and it was used to train the model. There are six different datasets that are used in the testing of the models' viability and performance. This paper offers a deep learning (DL) perspective, with the segmentation of brain MRI data serving as the only data source. The most cutting-edge developments in DL [19]

The fuzzy c-means clustering algorithms offer a lot of promise when it comes to extracting specific characteristics from picture pixels. One of the most prominent forms of unsupervised learning methods is fuzzy c-means clustering (FCM).Knowing the actual specifics of some of the factors, such as the quantity of clusters and the location surrounding the cluster centroid, is essential for the reason that the overall performance of the strategy relies upon on the input parameters. Several academics have issued warnings concerning a quantity of methods for counting clusters or cluster centroids [20][21]. Additionally, FCM frequently makes noise and gets caught in a neighbourhood. To prevent the fuzzy algorithm from being trapped in a nearby most excellent solution, many exclusive metaheuristic techniques have been used in its optimization of the goal characteristic. Additionally, FCM is unable to differentiate between objects in photos that have a comparable colour intensity when used on its own. To address the problems that were described, this study made use of the Gray Wolf Optimization (GWO) for the purpose of optimising [22]. The effectiveness of the cluster may be significantly boosted by using both FCM and GWO in tandem to locate the best possible cluster centers. The level of accuracy that each algorithm provides is the primary consideration that should be made when choosing the most appropriate algorithm for medical images. The subsequent goal in medical image processing is to simplify matters as much as possible. The objective of this inquiry is to integrate the FCM with the GWO as a consequence. By combining these two techniques, entrapment in close optima may also be avoided, and the cluster centres acquired from FCM may be further optimised. When examining breast cancer cytology pictures, the clustering will also make it simpler to separate the nucleus from the cytoplasm and other dark-colored cell characteristics [23]. Extreme learning machine (ELM) is an algorithm that was only recently invented. It is both speedy and effective, and it uses machine learning strategies to make accurate diagnoses of tumours in an extremely short amount of time. In a comparable vein, the significantly quick and strong fuzzy C-means clustering method, additionally recognised as FRFCM, is a cutting-edge approach that is both new and quick and is successful at exhibiting amazing overall performance. In this study, it is suggested that a method for segmenting brain tumours be used. The system's core consists of the extreme learning machine and the very rapid and strong fuzzy C-means clustering algorithms (BTS-ELM-FRFCM) that have been carried out on the Raspberry Pi (PRI) hardware [24]. We will talk about the strategy that supports the system

in the next section. The results of our suggested model are discussed in the next portion of the study. The morphological reconstruction of erosion and dilation is discussed in the next section, which may be found after this one. After that, the succeeding section contour detection using CAS and the contour angular section with FCM optimization were presented in detail.

Proposed Solution

Techniques are emphasized as the present architecture is then explored, with the focus being placed on how MRI Segmentation the use of DL methodologies has developed in notoriety over the years. The next section provides a more in-depth explanation of the recommended approach to the classification of brain tumours.

The Contour Angular Section (CAS) in Figure 1 is the proposed phase for the segmentation of MRI brain tumours the use of fuzzy C-Means optimization. . The following are some legitimate parts of the CAS algorithm:

Morphological Reconstruction process

RCE with FCM Optimization

RTS (Rotating Triangular Section) with FCM Optimization

CAS with FCM Optimization

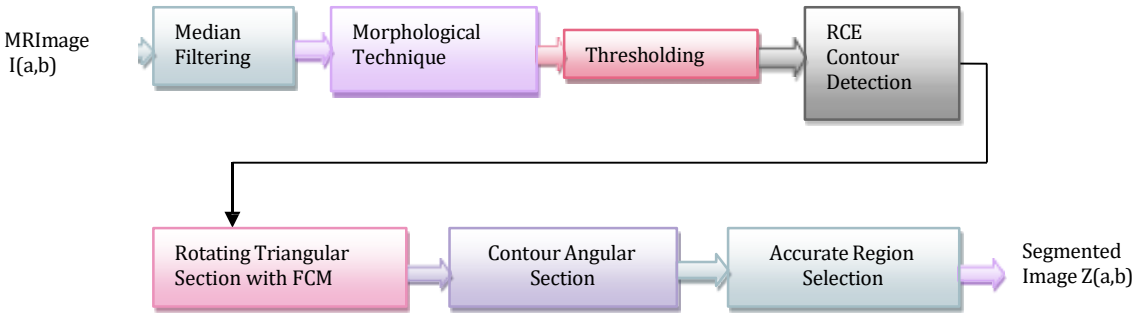

Figure 1: Proposed CAS with FCM- Block Diagram

To remove noise from a signal or image, let's preprocess the input MRI Picture I(a,b) using a median filter approach. The median filter is a non-linear digital filtering approach.. The median filter is essential in the realm of image processing for the reason that it is nicely regarded for its capacity to hold edges whilst additionally eliminating noise.The "window" approach, a method for intervening with the total entries using a median function, is a method used by the filter to evaluate each piece of incoming data. The window has a propensity to become more complicated when applied to signals with increasing dimensions. The range of medians in a constructing is decided by way of the whole variety of windows and is divided into two categories: odd and even. Use instead the median-filtered picture from the MRI Image (a,b) described in equation 1.

The median filter is a non-linear digital filtering technique that might also be used to eliminate undesirable noise from an image or sign. This filter can be applied to either an image or a signal. When a median filter is applied, the centre pixel of the neighbourhood is replaced with the pixel that represents the median of the neighbourhood. After thresholding the image that has undergone median filter processing, the background is removed using a two-level morphological reconstruction technique.Equation 2 describes the two-level morphological reconstruction procedure, which one may also use to guide their conclusions, T_0 is the threshold that is chosen when the Otsu threshold is used. The contour outside the area occupied by the tumor is established with the help of the output of the thresholder. The angular contour is subjected to the RCE technique as indicated in equation 2 to determine the tumour location. Let $Image_4(a,\ b)$ indicates the exterior masks contour surrounding the tumour region, which approximates the tumor's shape in contrast to the authentic tumour region's size, which $Image_4(a,b)$ used to be massive.

The FCM algorithm has successfully optimised this picture such that it may be used. In this picture, the outer contour of the area is getting an FCM optimization treatment based on the production of triangular sections. Instead of doing the FCM optimization on the full picture, we decided to do it separately. We begin by applying FCM optimization to each individual triangular zone, after which we partition the region that is encircled by the output of RCE into triangular regions. The result of FCM optimization includes objects of a much-reduced size. By using a precise area selection procedure, the smaller items may be removed from the scene.

Using the suggested contour angular section approach, further categorization of the different kinds and stages of brain

tumours may be accomplished in the future. Methods that are primarily based completely on convolutional neural networks (CNN) have the achievable to be used in the classification of a number types of cancers. The CNN based classification algorithm can additionally be used to instruct the traits of the tumour and the non-tumor vicinity due to the fact the novel approach that is motivated exactly segments the border vicinity of the brain tumour, which can give upup producing terrific Classification consequences.

Developing an algorithm for MRI brain tumour pictures that enables completely automated brain tumour identification and extraction is the goal of this model.

It is necessary for the detection algorithm to get rid of as much of the background as it can while still locating the tumour location.

The extraction technique should neither remove the pixels that represent the tumour, nor should it include the pixels that do not represent the tumour in the border area.

The innovative algorithm needs to have a better level of accuracy.

Algorithm 1: Algorithm for CAS-FCM

Step 1: Load the MRI images (a,b) into the median filtering programme.

This may be accomplished using the equation1,

$$Image_1(a,b) = \{MED\{I(a,b)\} \quad (a,b) \in w\} \qquad (1)$$

Step 2: In order to eliminate the backdrop, a 2-level morphological reconstruction technique is applied in equation 2.

$$Image_3(a,b) = \begin{cases} 1 \; if \; Image_2(a,b) \geq T_0 \\ 0 \; if \; Image_2(a,b) < T_0 \end{cases} \qquad (2)$$

The third step: T_0 is to choose a threshold shown in equation 3.

$$T_0 = \mu_{i1}(x_1) \times \mu_{i2}(x_2) \times \ldots \ldots \ldots . \times \mu_{in}(x_n) \qquad (3)$$

Step 4: Apply the RCE method to the angular contour.

Step 5: The FCM algorithm has been optimized.

Step 6: Apply FCM optimization to each triangle zone individually.

Step 7: Using the contour angular section technique, it is possible to further categorize the various types and stages of brain tumours.

Morphological reconstruction process

In the process of morphological opening, erosion often destroys smaller items, and the following dilatation frequently tends to restore the form of the larger structures that are left behind. However, the success of this restoration is contingent on the degree to which the forms and the structural element are comparable to one another. Opening by reconstruction, which is going to be covered in this part, is a procedure that brings back the original forms of the items that are still there after erosion. In morphological reconstruction, erosion and dilation are utilised as Levels 1 and 2, respectively. By eliminating the backdrop, the morphological reconstruction process reduces the non-tumor area. A block schematic of the two-level morphological reconstruction system is proven in Figure 2.

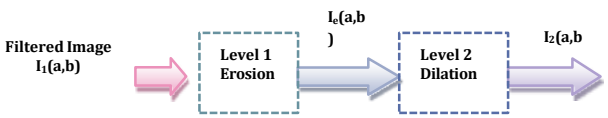

Figure 2: Morphological reconstruction process – Block Diagram

EROSION (Level 1)

The representation of erosion is Θ, it uses a structuring element for probing and reducing the shapes of the input image. The process or erosion of the mask image is created using the median filtered image $Image_1(x, y)$.Assume $M$is the mask's image and P is the marker image. The marker image's degree 1 masks image P can be expressed as follows: $r^e_{mask}(MI)$. Here $r^e_{mask}(MI)=e^{(n)}_{mask}(MI)$ with n such that $e^{(n)}_{mask}(MI)=e^{(n)}_{mask}(MI)$. Let $I_e(x,y)$ $I_e(x,y)$represents the eroded image or output of level 1.

DILATION (Level 2)

For the level 1 dilation procedure, an eroded picture $Imagee_e(a,b)$ is utilised as a mask image. Anticipate Q, which stands for the masks image, and M, which is the marker image, for the reason of simplicity. . The stage two masks image derived from the marker image M in this occasion may also be expressed as $r^d_{Qimage}(M)$, Here $r^d_{Qimage}(M)=d^{(n)}_{Q}(M)$ with n such that $d^{(n)}_{image}(M) = d^{(n+1)}_{Aimage}(M)$.

Let $Image(a,b)$shows the Dilation (level 2) output, image of Dilation, or two-level output of Morphological Reconstruction.

Where$\begin{bmatrix} 0 & 1 & 0 \\ 1 & 1 & 1 \\ 0 & 1 & 0 \end{bmatrix}$be the 3×3 matrix element of structuring used for level 2(dilation) and level 1(erosion).

Contour detection by CAS

The result of the thresholding operation is the contour detection of the CAS $Image_3(a,\ b)$. The region is selected by the CAS for FCM optimization. RCE, reveals the tumor's form. However, the RCE's size is greater than the initial tumor's. Figure 3 displays the block diagram for the CAS procedure.

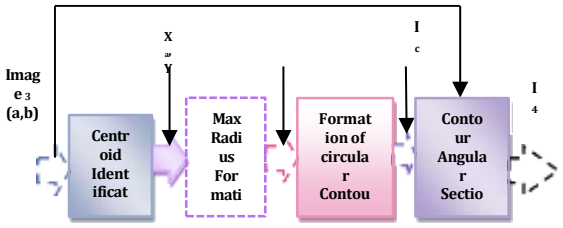

Figure 3: Block diagram of CAS

The contour angular process includes,

Identification - Centroid

Max- radius Estimation

Circular contour Formation

CAS

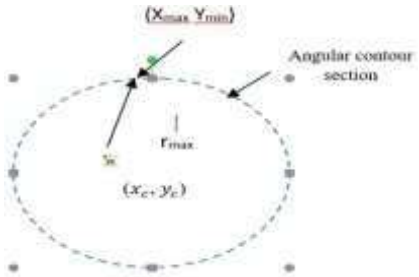

Figure 4: Centroid formation

Identification– Centroid

Let the $Image_3(a,\ b)$ be an image it contains background and foreground. The picture's background depicts the background area and the foreground image region, with the centroid of the location approximated. $(x_\alpha,\ y_\alpha)$Be the centroid pixel that used to be determined via the centroid identification process shown in figure 4.

Let's NUM_1 express the function of the edge pixels and let's$(a_1,\ b_1),\ (a_2,\ b_2),\ \ldots\ \ldots\ (a_{N1},\ b_{N1})$ estimate the differ of edge pixels in the thresholded image and let $(a_1,\ b_1),\ (a_2,\ b_2),\ \ldots\ \ldots\ (a_{N1},\ b_{N1})$ symbolize the feature of edge pixels. Let $(x_\alpha,\ y_\alpha)$ characterize the centroid that is supplied by the thresholded image. The edge pixels are often proven as $(a_i,\ b_i)\ i = 1,2,\ldots N1$ From the edge pixels the centroid man be calculated in equation 4,5,6 as

$$(X_a, Y_b) = (\frac{a_1+a_2+\cdots+a_{N1}}{N1}, \frac{b_1+b_2+\cdots b_{N1}}{N1}) \quad (4)$$

The centroid can also be expressed as

$$a_x = \frac{1}{N1}\sum_{i=1}^{N1} a_i \quad (5)$$

$$b_y = \frac{1}{N1}\sum_{i=1}^{N1} b_i \quad (6)$$

B. MAX - RADIUS ESTIMATION

The region of edge pixels $(a_1, b_1), (a_2, b_2), \ldots\ldots (a_{N1}, b_{N1})$ and the centroid (x_a, y_a) , locate the radius of each edge pixel $r_1, r_2 \ldots\ldots r_{N1}$ the usage of the relation in eq 7

$$r_i = \sqrt{(a_x - a_y)^2 + (b_x - b_y)^2} \quad (7)$$

From the $N1$ quantity of radii r_i , estimate the maximum radius the usage of the equation 8,

$$r_{max} = \max(r_1, r_2, \ldots\ldots r_{N1}) \quad (8)$$

Let (x_{max}, y_{max}) represent the positions of the edge pixels with the maximum r_{max} as shown in figure 5, figure 6.

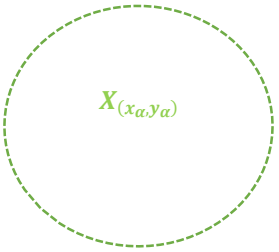

Figure 5: Max - Radius estimation

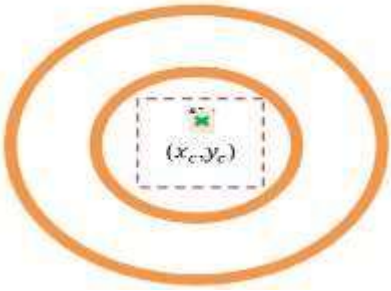

Figure 6: Formation of Contour Angular

C.FORMATION OF ANGULAR CONTOUR

Create a circle inside the image $I_3(a,\ b)$ using the maximum radius r_{max} and the centre pixel $(x_a,\ y_a)$ to produce the circular contour image. Through the potential of the circular shape, the whole tumour region is now completely encircled. In areas of good quality, the edge pixel is pretty close to to the circular contour's radius $r_i \approx r_{max}$. There are quite a few areas the place the edge pixel isn't always typically pretty shut to the circular contour the place the radius is, even though $r_i \ll r_{max}$. To gain the purpose of making the outer contour's shape fit the structure of the tumour site, we might also additionally use the RCE approach to the circular contour. Radius contraction, normally referred to as RC, reasons the circular development to cross in the direction of the Region of Interest (ROI). Every pixel placed on the circular contour will experience the radius contraction.

(d) Contour Angular Section

In contour angular section, the first step is the contraction of the radius, and the second is the expansion of the contour. The reduced contour edge pixels may be 52222

determined using the formula in equation 9,

$$(u_i^*, v_i^*) = \left(\frac{x_i \pm X_i}{2}, \frac{y_i \pm Y_i}{2}\right) \quad (9)$$

The distance between (x_i, y_i) and $(u_i, v_i)$is calculated in equation 10,

$$d_i = \sqrt{(x_i - u_i)^2 + (y_i - v_i)^2} \quad (10)$$

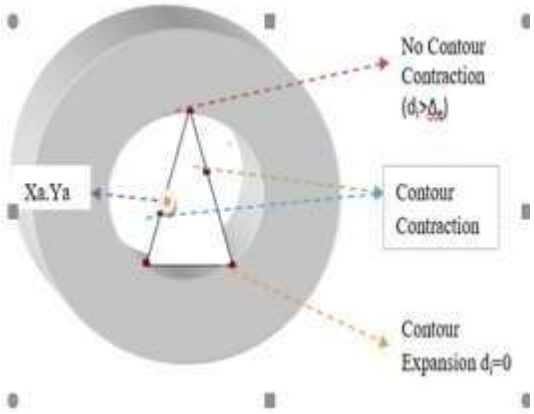

Figure 7: Contour Angular Section

The condition $d_i < \Delta_e$ is met by the contracted contour edge pixels, so those pixels are the ones that get expanded. Radius expansion (RE) is carried out utilising an expansion threshold after RC (Radius Contraction) (Δ_e). If the distance between $(x_i,\ y_i)$ and $(u_i,\ v_i)$ is less than the expansion threshold, the new contour edge pixel expands. Figure 7 shows the block diagram of RTS with FCM Optimization.

Contour Angular Section with FCM Optimization

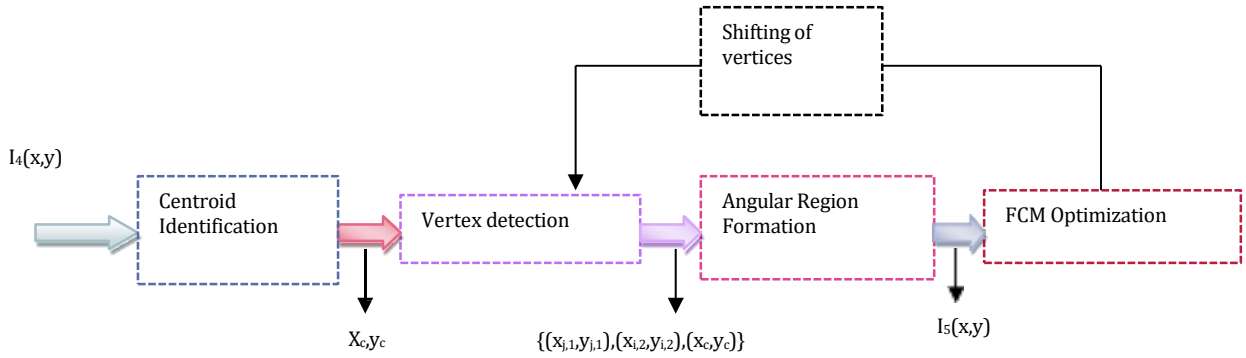

Figure 8: Section with FCM optimization Block Diagram

Let$I_4(a,\ b)$ be the region that was segmented by Contour Angular Section process, and it is shown in figure 8. The FCM optimization for edge pixels that can be regarded to be tumour region. To apply FCM, the tumour area was separated into small rectangular sections. The triangular region selection is an iterative process. The following are the steps concerned in contour angular section with FCM optimization in figure 8,

Formation of Centroid

Detection of Vertices

Formation of Triangular region

FCM optimization

Formation of Centroid

Let the vary of part pixels be targeted thru and the vicinity of part pixels be represented by using utilising RCE in the contour computed the use of $(a_1,\ b_1)$, $(a_2,\ b_2)$, ... $(a_{N2},\ b_{N2})$. Let $(x_c,\ y_c)$ indicate the RCE-estimated contour's centroid. Generally, $(a_i,\ b_i)i\ =\ 1,2,$ ... ... $N2$ are represented as edge pixels and it is shown in figure 9. From the edge pixels, the centroid may be calculated in equation 11,

$$(x_c, y_c) = (\frac{a_1+a_2+\cdots+a_{N2}}{N2}, \frac{b_1+b_2+\cdots+b_{N2}}{N2}) \quad (11)$$

The centroid can also be expressed in equation 12,13

$$x_c = \frac{1}{N2}\sum_{i=1}^{N2} a_i \quad (12)$$

$$y_c = \frac{1}{N2}\sum_{i=1}^{N2} b_i \quad (13)$$

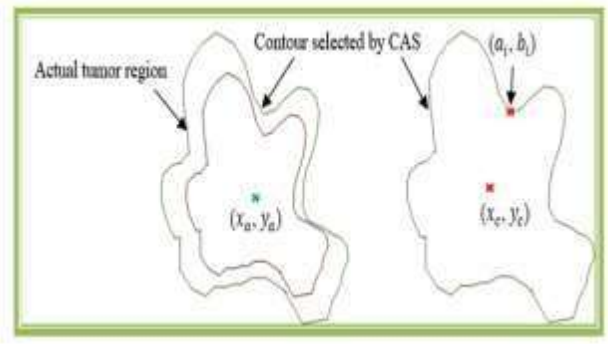

Figure 9: Estimation of Centroid from the Contour selected by CAS

(b). Detection of vertices

Let $(x_{j,1},\ y_{j,1})$ be a contour selected pixel by CAS and $(x_{j,2},\ y_{j,2})$ be a one of a kind pixel in the contour spaced at S the place S denotes the spacing aspect. The number of pixels between $(x_{j,1},\ y_{j,1})$and$(x_{j,2},\ y_{j,2})$ plus one using space factor shown in figure 10.

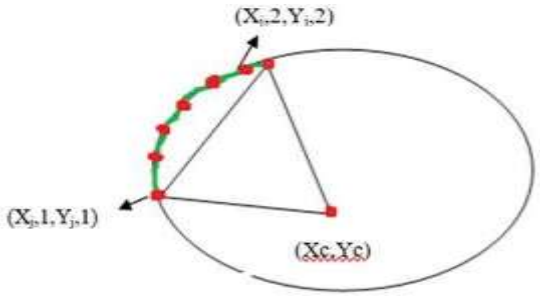

Figure 10: Vertices detection

(c) Angular region formation

Using the pixels$(x_{j,1},\ y_{j,1}\ )$, $(x_{j,2},\ y_{j,2})$ and$(x_c,\ y_c)$. At the vertices, a triangle-shaped zone is formed.. Let $I_{1,T}(x,\ y)$ be the region of triangular section. The triangular portion area rotates clockwise for each iteration. Let $I_{1,T}(x,\ y)$ be the region of the triangle created by the vertices $(x_{1,1},\ y_{1,1})$, $(x_{1,2},\ y_{1,2})$ and $(x_c,\ y_c)$. Similarly, $I_{2,T}(a,\ b)$ be the region of triangle formed by the vertices $(x_{2,1}, y_{2,1})$, $(x_{2,2}, y_{2,2})$and $(x_c, y_c)$and so on.

(d) FCM optimization

Once the triangular vicinity issue has been selected, the pixels inside the triangle region area are optimised the use of the fuzzy C- Means method. Fuzzy C-Means manner output eliminates non-tumor pixels and returns the tumour pixels. Let $I_{j,T}(x, y)$ be a triangle with a certain amount of N_3 pixels; shown in eq 14,

$$P_k = \{P_1, P_2, \dots\dots\dots P_{N_3}\} \quad k = 1,2, \dots\dots\dots N_3 \qquad (14)$$

Let N_c point out how many cluster pixels are used in the FCM approach. The FCM technique is divided into two cluster pixels in this occasion $N_c = 2$. The membership of each pixel P_i set must be M_{il} for any cluster l. Let be the pixel between 0 and 1, the cluster centreC_l of l, and the discarded value δ for which the clustering is finished. Both the fuzziness index (F) and the number of iterations (N_F) are actual numbers larger than one. The FCM is used to optimise the pixels in the TS (Triangular Section) in the manner described below.:

Step 1: Let $M^{(0)}$ be the membership initially

Step 2: where M represents the membership matrix and$M = M_{il}$

Step 3: The center's matrix for any iteration t is shown as, $Cet^{(t)} = [C_l]$

$$C_l = \frac{\sum_{l=1}^{N_C} M_{il}^F P_i}{\sum_{l=1}^{N_c} M_{il}^F} \qquad (15)$$

Step 4: Utilizing the cluster, update the membershipC_l,

$$M_{il} = \frac{1}{\sum_{t=1}^{N_F} \left(\frac{d_{il}}{d_{tl}}\right)^{\frac{2}{F-1}}} \qquad (16)$$

$$d_{il} = \sqrt{\sum_{i=1}^{N2} (P_i - C_l)} \qquad (17)$$

Step 5: Steps two through three should be followed up until the termination rate or a significant cost is reached between the membership of two future iterationsδ.

$$||M^{(t)} - M^{(t+1)}|| \geq \delta \qquad (18)$$

Step 6: If $||M^{(t)} - M^{(t+1)}||$is less than the final amount in value δ,

Step 7: Stops the iteration process.

The distance to the cluster and its depth outline every pixel's region in the image..The pixel P_i, will have a increased membership in the opposing cluster if there is a massive gap between the cluster centre and it. The FCM-optimized triangular section is $I_4(a, b)$. There may be minor sections in the FCM-optimized picture $I_4(a, b)$ that can be removed to get an accurate segmented output $Z(a, b)$.

Experimental results

Figure 11 shows the experimental consequences and an evaluation of the proposed approach.

Dataset

We assessed the effectiveness of the recommended brain tumour segmentation approach to the use of test images from the T1-weighted contrast-enhanced picture collection [20] using MATLAB. There are 233 individuals in this dataset with one of three different forms of brain tumours: meningeal, glioblastoma, or hypophysis. The collection includes 930 slices of tumor images of the hypophysis, 708 slices of glioblastoma, and 1426 slices of meningeal tumor images. As a result, this dataset, which is used to consider the effectiveness of the recommended methods, has a total of 3064 slices.

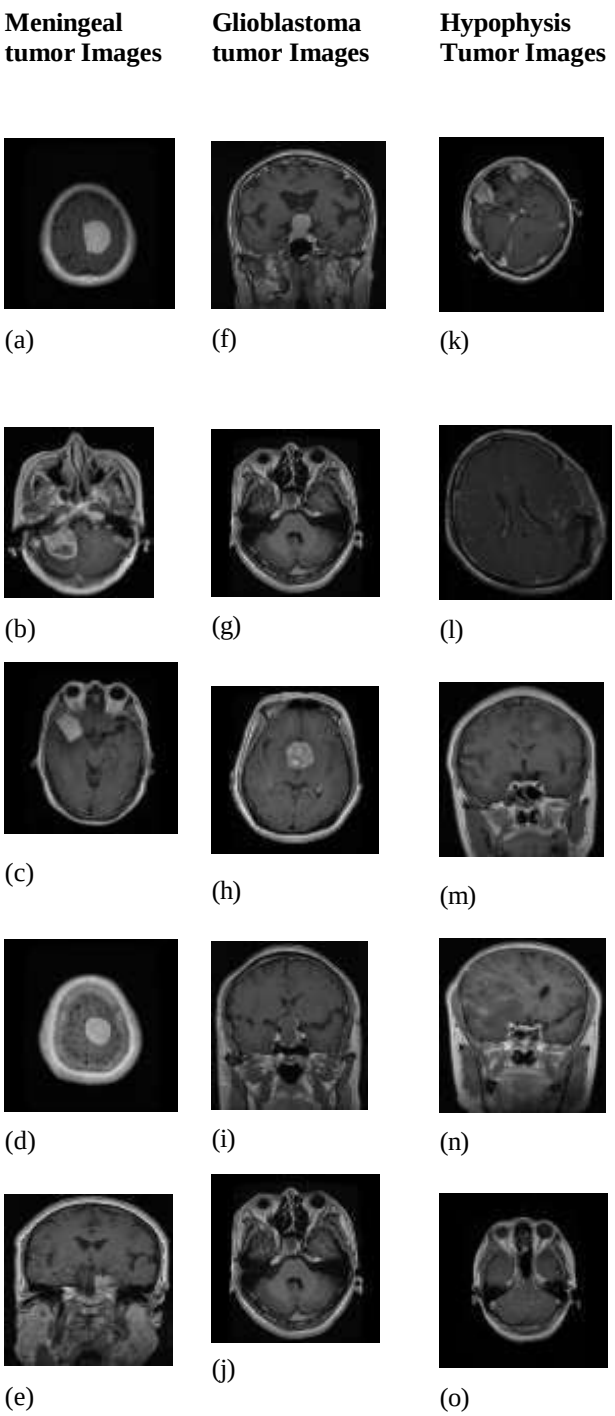

Figure 11 Examples of test MRI images from a tumor dataset with various forms of weighted contrast enhancement (a)-(g) Meningioma ,(h)-(n) Pituitary tumor, (o) Glioma

The collection contains MRI tumour photographs with a resolution of 512 by 512 and a bit depth of 16, and each image includes ground truth information such as a tumour mask and a tumour boundary. The ground truth tumour mask is depicted in Figures 12(a) and (b) as a binary image with 512 by 512-pixel dimensions, a logic value of one to indicate the presence of a tumor, and a logic value of zero to indicate the absence of a tumor. The coordination of the border pixels might also be used to determine the proper placement of the tumour borders. Because the dataset (the team of experts) provided the ground truth result, validating the conclusion of the proposed task is a rather straightforward process. It is not necessary to get the findings validated by a group of medical professionals.

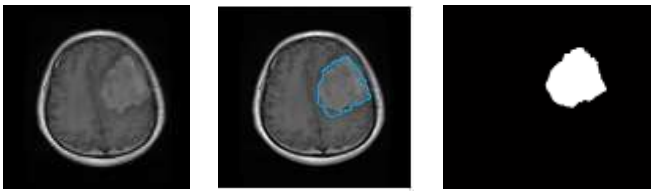

(a) (b) (c)

Figure 12 Sample test image and the results of the ground truth (a) Sample image (b) indicated by blue color (Ground truth tumor boundary) (c) The tumour is displayed in the white zone, while the non-tumor is displayed in the black region (Ground truth – tumour mask).

Measures which include Specificity, Sensitivity, Dice-Score (DS), Probabilistic Rand Index (PRI), and HausdorffDistance(HD) have been used to examine the overall performance of the two techniques that had been cautioned. Assume that the phrases T_p, T_n, F_p, and F_n, which stand for true positive, proper negative, false positive, and, correspondingly, false negative, characterize the parameters. The output of the segmentation algorithm contrasts with the ground truth give-up end result from the database to decide these parameters. The segmentation cease end result is diagnosed as a true negative (Tn) if the output of the segmentation method and the segmentation quit end result each resemble a tumour in the actual world. If the output of the segmentation method and the segmentation end result are both comparable to tumours, the classified result is acknowledged as a true positive (T_p) in expressed eq in 19

$$Specificity\ (S_p) = \frac{T_n}{F_p+T_n} \quad (19)$$

The measure of positives that are detected as incorrectly positives, or true positive rate, is another way that sensitivity is expressed in eq 20.

$$Sensitivity\ (S_e) = \frac{T_p}{F_n+T_p} \quad (20)$$

The dice score (DS) shows how the segmentation output of the suggested method matches the actual results. The relation, which can be used to estimate the dice score (DS) in eq 21,

$$Dice\ score\ (DS) = \frac{2T_p}{F_p+2T_p+F_n} \quad (21)$$

The proportion of combinations between the segmentation output and the floor reality findings whose labelling, such as tumour and non-tumor, is often diagnosed as the PRI (probabilistic Rand Index). The PRI value is between 0 and 1. If the segmentation technique is more likely the worst, then PRI=0 shows that the segmentation implications are significantly different from the ground truth consequences. The value of PRI = 1 suggests that the segmentation method is extraordinarily accurate if the segmentation and floor truth outputs are same. The PRI (Probability Rand Index) may be calculated using this relationship in eq 22.

$$PRI = \frac{A_1+A_2}{A_1+A_2+B_1+B_2} \quad (22)$$

The difference between segmented pixel results and those represented by the expression $B_1 + B_2$ is demonstrated by the suggested algorithm and the ground truth final result , as well as the similarity between the proposed algorithm's pixel segmented end result and the ground fact end result is represented through way of the expression $A_1 + A_2$.

The Hausdorff distance, which offers the biggest difference in tumor sizes, can be used to estimate the most surface distance. Assume that the ground truth-supplied segmentation result is provided as G and the algorithm's segmentation result is H. Using the relation, one can estimate the Hausdorff distance shown in eq 23

$$HD = \max\{Ha(G,H), Ha(G,H)\} \quad (23)$$

where,

$$Ha(G,H) = \max_{x\in H} \min_{y\in G} |a-b| \quad (24)$$

An very close match between the segmentation and ground reality repercussions is shown by less Hausdorff distance (HD). We consider our suggested strategy using the metrics DS (Dice-Score), Sp (specificity), Se (sensitivity), PRI, and HD (Hausdorff Distance).

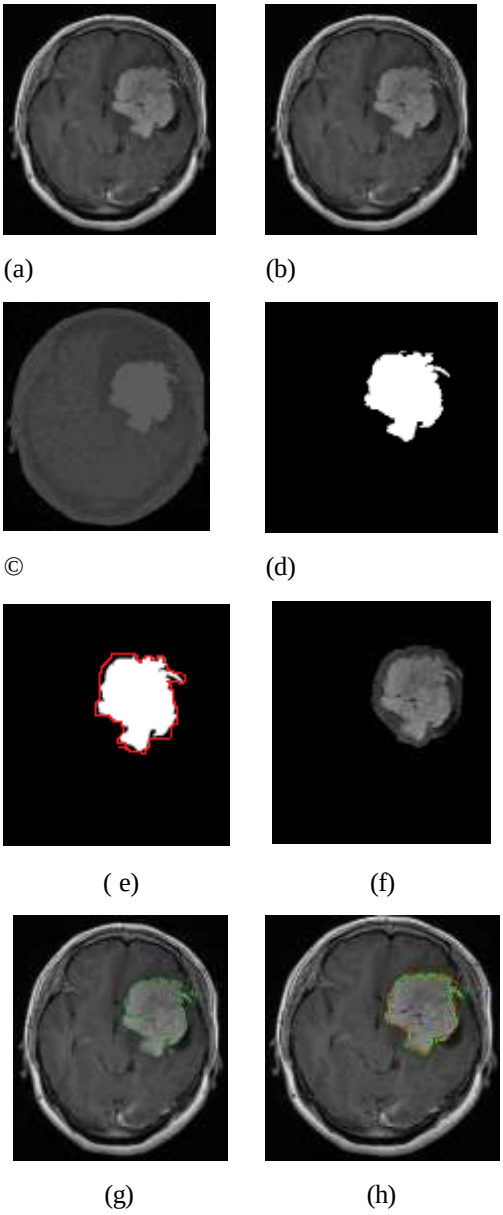

Figure 13 Meningeal kind tumor Experimental consequences (a) Input MRI Image (b) Filtered image the usage of Median Method (c) a two-level, morphologically recreated image (d) Thresholded image (e) RCE technique (f) Output after CAS (g) contour angular section based FCM (h) Proposed segmentation output

Figure 13 shows the experimental outcomes for the meningeal tumour kind. In Fig. 13(e), the circular contour is depicted in blue, the radius of the contour is depicted in green, and the prolonged contour is depicted in red. The proposed ground truth result (shown in green) and the segmentation findings are shown in Fig. 13 (h) (red color).

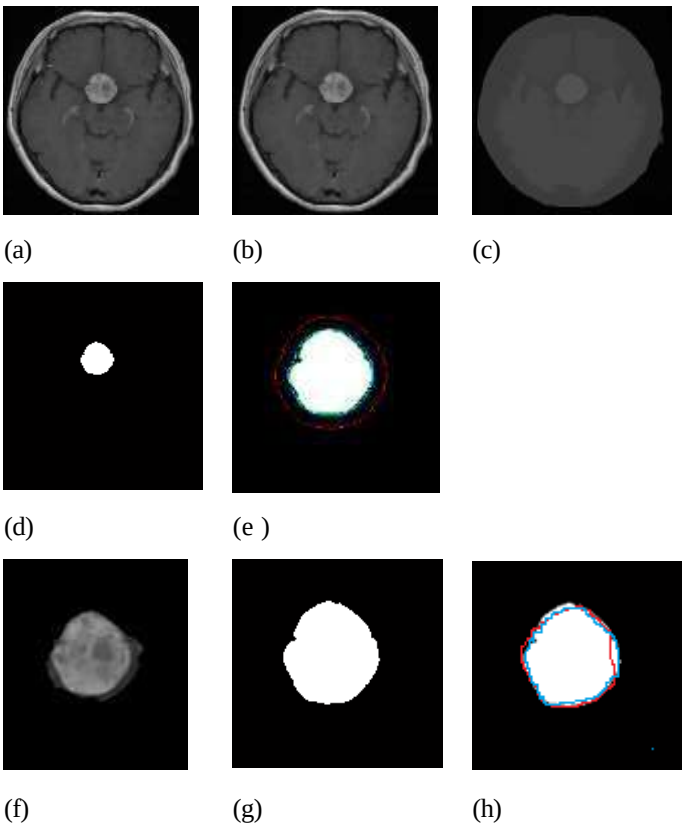

Figure 14 Pituitary Tumor type Experimental consequences (a) Input MRI Image (b) Filtered image the utilization of Median approach (c) Two stage morphological reconstructed image (d) Thresholder image (e) CAS approach (f) Output after contour angular section CAS (g) contour angular based totally FCM (h) Proposed segmentation output

Figure 14 depicts the experimental findings for the pituitary tumour type. In Fig. 14(e), the expanded contour is shown in pink, the radius is shown in green, and the round contour is shown in blue. The planned segmentation result (shown in Green color in Fig. 14(h))) and the actual results are shown (red color).

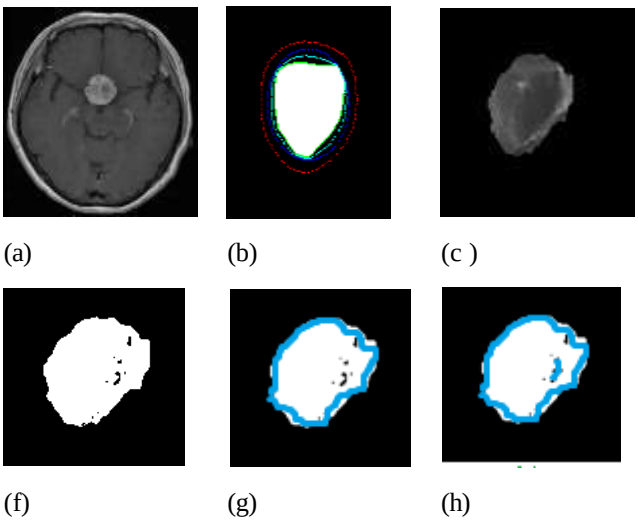

Figure 15 Tumor kind Glioblastoma Experimental effects (a) Input MRI Image (b) RCE device (c) CAS Output (d) FCM output (e) Region selection input (f) output for proposed segmentation

The experimental findings for the tumor kind glioblastoma are proven in Figure 15. In figure 15(b), the circular contour is depicted in blue, the radius is depicted in green, and the prolonged contour is depicted in pink. Figure 15(f) displays the

projected segmentation result (shown in green) and ground truth findings (red color).

Modern techniques, which consists of LACM [14], DNN [15], Multimodal MRI [16], MC-CNN [25], Survival prediction [26], and our in the previous efforts, Greedy [27], Radius Contraction and Expansion (RCE)[28], and RTS[29], have been examined, as top as the universal overall performance of the recommended method.

The effectiveness of the two advised algorithms used to be once assessed the use of measures such

Dice Score

Sensitivity

Specificity

Hausdorff distance

Probabilistic Rand Index

These parameters are calculated via matching or contrasting the segmentation algorithm's output with the database's ground truth result. The segmentation output of the recommended technique is matched with the ground reality findings the use of Dice Score (DS) was shown in eq 21.

Table 1 Dice score contrast of the cautioned technique and state-of-the arts strategies

Tumor Types	LACM	DNN	Multimodal MRI	MC-CNN	Survival Prediction	Greedy	RCE	Rotating Triangular Section	Proposed Method
Meningeal	0.9	0.87	0.92	0.94	0.94	0.96	0.975	0.991	0.994
Glioblastoma	0.9	0.88	0.92	0.92	0.93	0.94	0.962	0.98	0.99
Hypophysis	0.89	0.87	0.9	0.9	0.91	0.91	0.935	0.957	0.968

When compared to the conventional technique, the suggested method has high dice score values for three different tumour kinds, as indicated in table 1. Meningeal, glioblastoma, and hypophysis have been observed to have dice rankings of 0.994, 0.99, and 0.968, respectively. The graphic evaluation of the dice-score of the cautioned technique and the traditional strategies is proven in Figure 16. The proposed method's average Dice-score was 0.984.

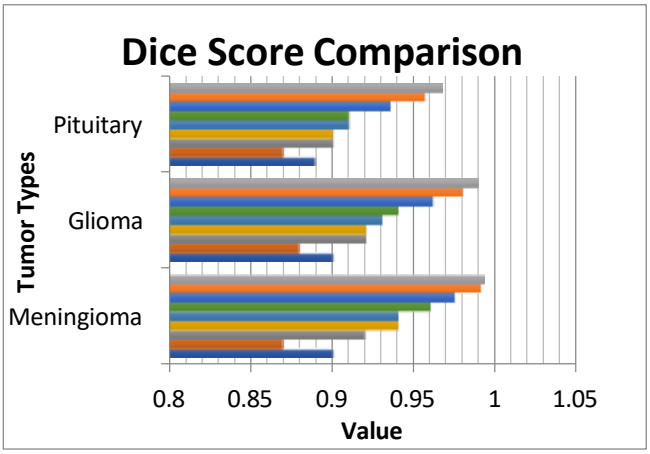

Figure 16 Dice scores from the suggested method and those from cutting-edge methods are compared.

Table 2 compares the recommended method's sensitivity to the traditional procedures for three distinctive sorts of cancers. Sensitivity values for meningioma, glioma, and the pituitary had been mentioned to be 0.78, 0.63, and 0.56, respectively. Figure 17 visually compares the Sensitivity of the suggested method to the traditional procedures. The average sensitivity of the suggested approach was to be 0.657.

The measure of positives that are detected as incorrectly positives, or true positive rate, is another way that sensitivity is expressed in equation 20.

Table 2 using cutting-edge methods to assess the suggested approach's sensitivity

Tumor Types	LACM	DNN	Multimodal MRI	MC-CNN	Survival Prediction	Greedy	RCE	Rotating Triangular	Proposed Method
Meninge	0.6	0.58	0.6	0.62	0.64	0.67	0.71	0.78	0.81
Glioblastoma	0.43	0.41	0.45	0.47	0.49	0.51	0.55	0.63	0.70
Hypophysis	0.36	0.35	0.38	0.4	0.42	0.44	0.49	0.56	0.64

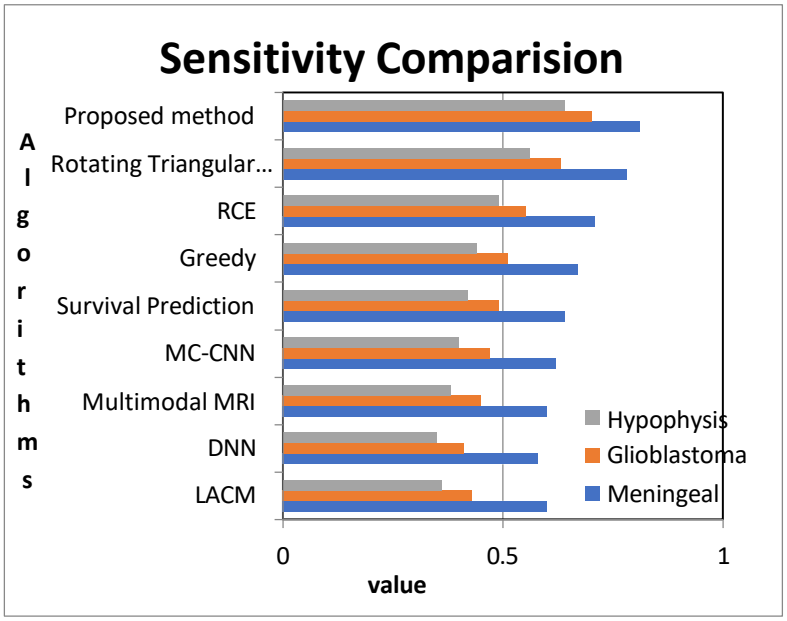

Figure 17 Comparison of the suggested method's sensitivity to current best practices

For three distinct tumour forms, along with meningiomas, pituitary tumours, and gliomas, Table 3 compares the specificity of the recommended approach with the standard strategies. The reported specificities for meningioma, glioma, and pituitary were 0.86, 0.71, and 0.61, respectively. In Figure 18, the new method's sensitivity is visually distinctive to the ordinary techniques. The common sensitivity of the recommended technique used to be once 0.727

A alternative indicator for specificity is the true negative rate, which counts the percentage of false negatives that are precisely recognized in equation 19.

Table 3 Specificity assessment of advised method the use of contemporary methodologies

Tumor	LACM	DNN	Multimodal MRI	MC-CNN	Survival Prediction	Greedy	RCE	Rotating Triangular Section	Proposed Method
Meningioma	0.67	0.65	0.69	0.72	0.75	0.78	0.825	0.86	0.89
Glioma	0.52	0.49	0.52	0.54	0.57	0.59	0.64	0.71	0.76
Pituitary	0.42	0.4	0.42	0.45	0.47	0.49	0.53	0.61	0.69

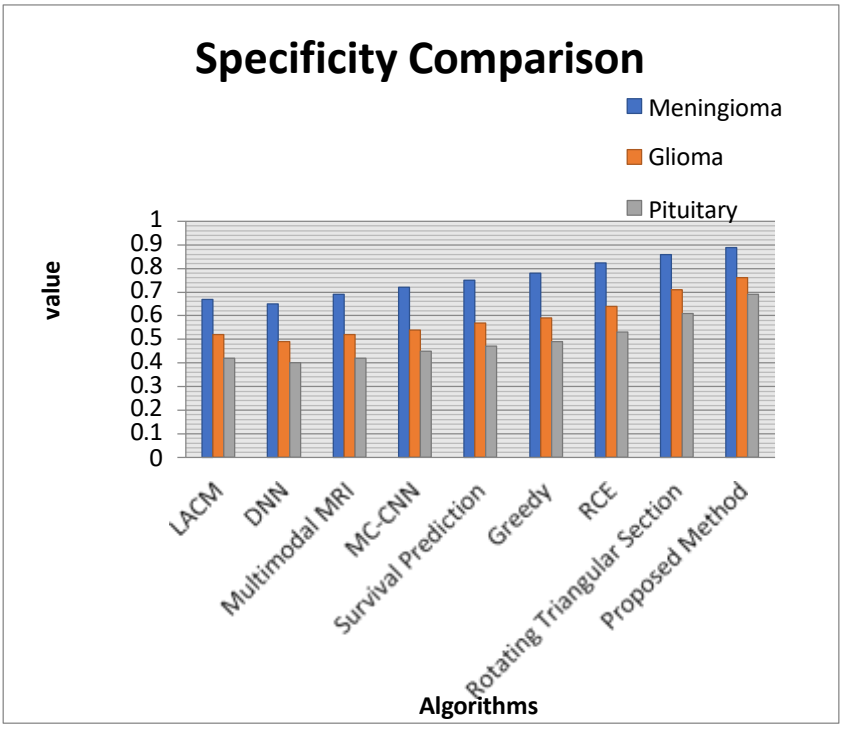

Figure 18 Comparison between proposed method with present day in phrases of specificity

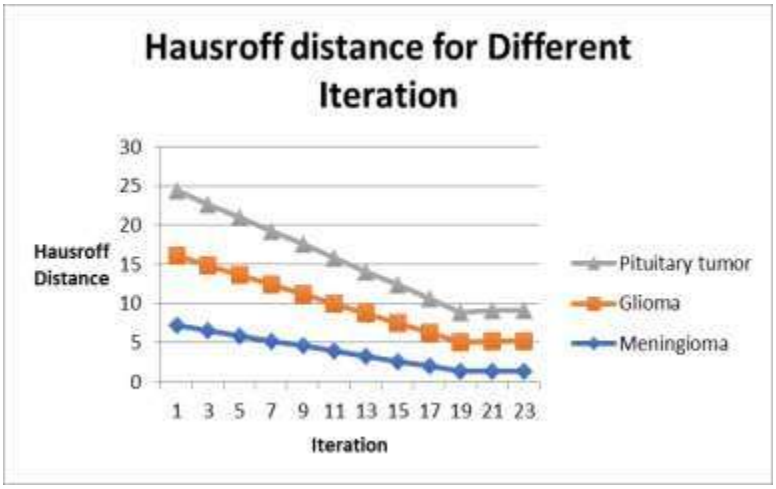

Figure 19 Hausdorff distance for different iteration

Figure 19 illustrates the variance in Hausdorff distance for various tumour shapes and iterations. The Hausdorff distance decreases as the number of repeats rises. This demonstrates how well the final segmentation result fits the output.Meningiomas have a lesser Hausdorff distance than gliomas and pituitary tumours when the Hausdorff distances of three distinct tumour types are compared. Table 4 suggests the Hausdorff distance value in proportion to the quantity of iterations. The Hausdorff decreases throughout the iteration, and when it reaches its minimum value, the iteration is complete. The Hausdorff distance measure, which distinguishes between tumour sizes with the greatest precision, may also be used to estimate surface distances to the greatest extent. More thorough matching between the segmentation and ground truth findings is indicated by a lower Hausdorff distance shown in equation 23 and 24.

$$HD = \max\{Ha(G,H), Ha(H,G)\} \quad (23)$$

$$Ha(G,H) = max_{x\in H} min_{y\in G} |x-y| \quad (24)$$

Table 4 Hausdorff distance for different iteration

Iteration	1	3	5	7	9	11	13	15	17	19	21	23
Meningeal	7.2	6.55	5.9	5.25	4.6	3.95	3.3	2.65	2	1.35	1.37	1.3889
Glioblastom	8.9	8.333	7.776	7.179	6.662	6.055	5.488	4.911	4.334	3.777	3.886	3.887
Hypothesis	8.332	7.822	7.332	6.822	6.332	5.822	5.332	4.822	4.332	3.822	3.90	3.91

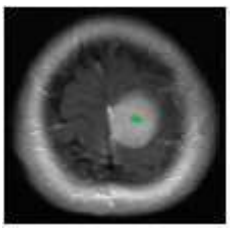

(a)

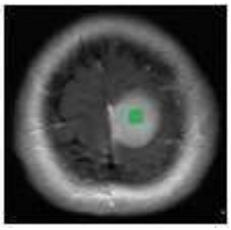

(b)

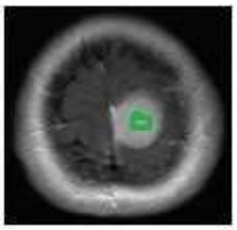

(c)

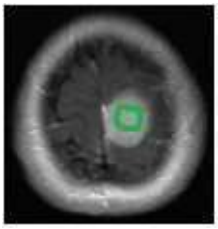

(d)

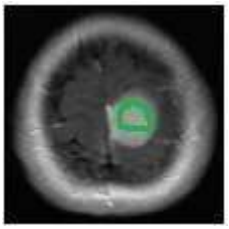

(e)

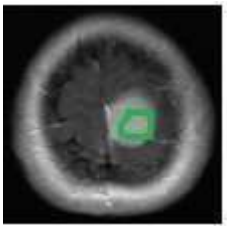

(f)

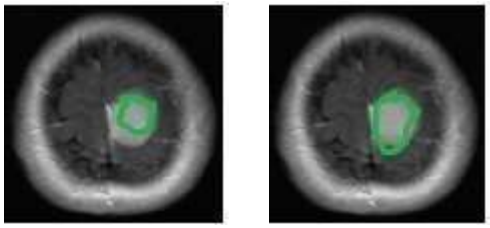

(g) (h)

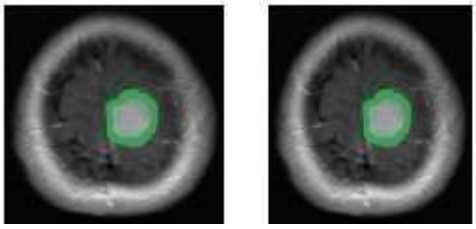

(i) (j)

Figure 20 Different spacing factor and its Segmentation result (a) Input image (b) $S = 45$(c) $S = 40$ (d)$S = 35$ (e) $S = 30$(f) $S = 25$(g) $S = 20$ (h) $S = 15$(i) $S = 10$

The segmentation output for a variety of spacing elements is shown in Figure 20. If the edges are not correctly divided because of the aliasing issue, the spacing factor is likely large. When the spacing element is lower, the edges segment correctly.

Table 5 Hausdorff distance while using various spacing factors

Spacing Factor	5	10	15	20	25	30	35	40	45	50	55	60
Meningioma	1.4	1.35	1.42	1.53	1.64	1.72	2.13	2.68	2.92	2.93	2.98	3.02
Glioma	3.8	3.77	3.85	4	4.1	4.2	4.3	4.5	4.7	4.8	4.9	4.9
Pituitary	3.88	3.82	3.9	3.98	4.1	4.21	4.4	4.64	4.9	4.9	5.01	5.08

Figure 21 suggests the fluctuation of the Hausdorff distance for a wide variety spacing factors for a range of tumour kinds. The Hausdorff distance grows as the spacing component grows. This implies that when the spacing thing decreases, the segmentation stop end result carefully displays the floor reality end result. If the spacing component is high, then the Hausdorff distance is too top notch. As viewed in table 4, when evaluating the Hausdorff distance of three distinct tumour types, meningiomas have a smaller Hausdorff distance than gliomas and pituitaries.

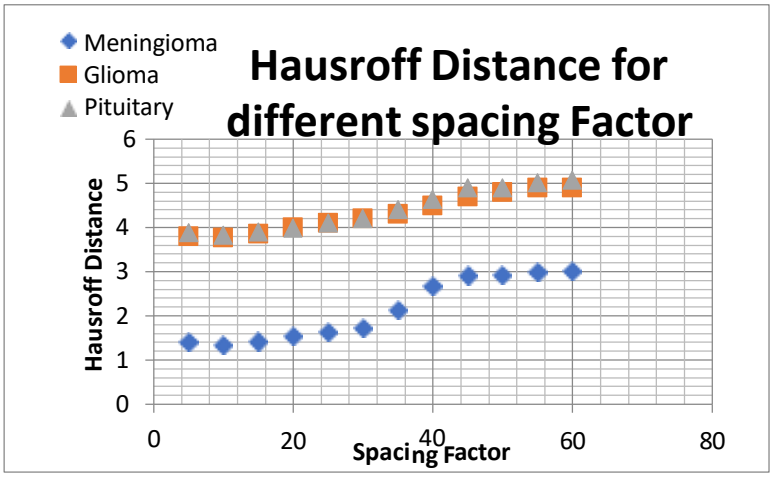

Figure 21 Hausdorff distance for various spatial factor

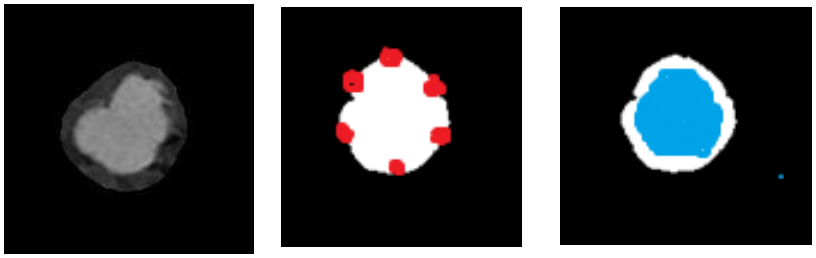

(a) (b) (c)

Fig 22: Results of the Rotating Triangular Section with FCM Optimization Experiment: (a) output after radius growth and contraction (b) space between triangles all through formation (c) FCM output primarily based on rotation of the triangles

Figure 22 shows the outcomes of the CAS experiment utilising the FCM optimization technique. The consequences of the RCE manner are proven in Fig. 25(a), and Fig. 25(b) indicates the contour's chosen vertices for angular improvement with a separation problem of $S = 10$. Fig 22 (c) demonstrates the tumor's segmentation inside the RCE (Radius Contraction and Expansion) contour region.

The segmentation output and the proportion of pairings between the ground truth penalties whose labelling, such as tumour and non-tumor, are regular are characterised as the PRI. The difference between PRI levels zero and one. If there are no similarities between the segmentation findings and the ground truth, the PRI value is zero. If they are the same, the PRI value is 1.

Table 5 PRI A comparison between the suggested approach and our earlier work

	Meningioma	**Glioma**	**Pituitary Tumor**
Greedy Snake [26] without FCM	0.9124	0.9234	0.8932
Greedy Snake [26] without FCM	0.9684	0.9532	0.9321
RCE [27] without FCM	0.9372	0.9415	0.9106
RCE [27] with FCM	0.9783	0.9672	0.9499
Triangular Section without FCM	0.9578	0.9502	0.9302
Triangular Section with FCM	0.9912	0.9742	0.9572
Contour Angular Section without FCM	0.9665	0.9605	0.9305
Contour Angular Section with FCM	0.9952	0.9833	0.96674

The PRI comparison between the suggested technique and our works on the Greedy Snake Algorithm [27], Radius Contour and Expansion [28], and RTS [29] is shown in Table 5. The recommended strategy can provide PRI values of 0.9912, 0.9742, and 0.9572, respectively, for the malignancy's meningioma, glioma, and pituitary tumour.. In addition to using FCM optimization, the suggested technique yields PRI values of 0.9578, 0.9502, and 0.9302 for the tumours meningioma, glioma, and pituitary tumour, respectively.. Figure 23 shows that the suggested method's average PRI is higher than our previous study, at 0.9742.

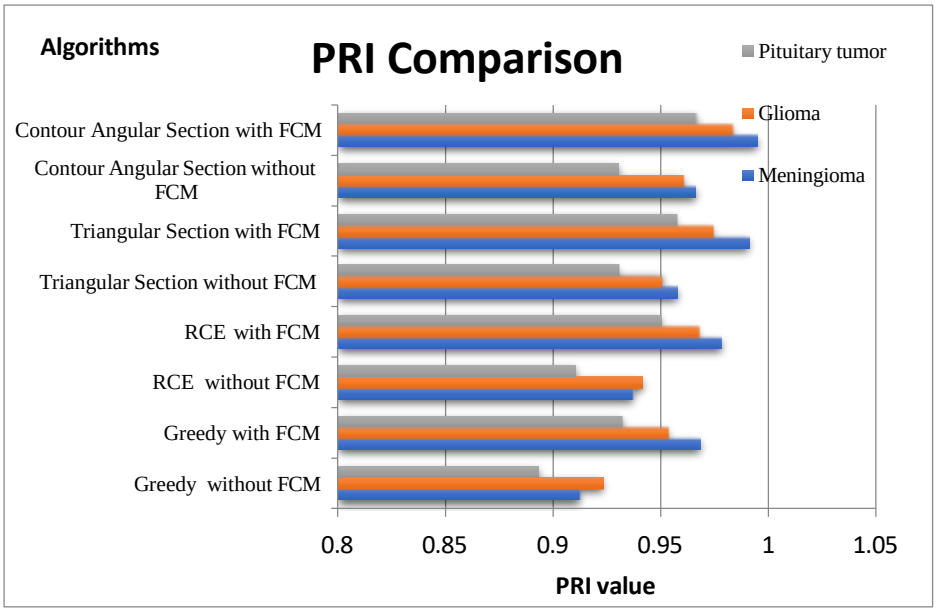

Figure 23 Comparison of the previous work with PRI

3. CONCLUSION

This study provided a brand-new contour angular section with an algorithm for segmenting brain tumours based on the FCM approach. The background is removed from MRI images using the median filter approach, two-level thresholding methods, and morphological reconstruction. The tumour site is then chosen for FCM optimization utilising a system of location contraction and expansion. By producing a circular contour, the place of contour contraction and expansion is determined. The size of the circular contour is expanded and contracted to obtain an approximate tumour region. Using the RCE approach, a triangular area is created by removing the vertices from two contour pixels and the centroid pixel. To obtain the triangular region, the FCM is applied to get an optimised segmentation result. The FCM is then utilised as soon as possible to reach the location created by the clockwise movement. This gadget is continued until the triangular segment completes one full rotation. For three exclusive cancers—meningioma, glioma, and pituitary—the experimental consequences are evaluated the use of metrics such cube score, sensitivity, specificity, the probabilistic Rand index, and the Hausdorff distance. Calculated values for the frequent dice score, sensitivity, specificity, and PRI are 0.656, 0.726, 0.976, and 0.9742, respectively. These metrics are more sophisticated than the traditional approaches. The PRI of meningioma, glioma, and pituitary tumours used to be before decided to be 0.9912, 0.9742, and 0.9572, respectively, in accordance to the [27], [28], and [29] techniques. The greater PRI value suggests a sturdy correlation between the proposed segmentation end result and the actual findings. Depending on the spacing factor, the iteration of the contour angular FCM rises as the Hausdorff distances reduce. A suitable segmentation is produced via lowering the factor, which produces an exact segmentation at the borders. The Hausdorff value is less than 4.5, which is lower than what can be obtained using conventional techniques. The proposed method outperforms more established techniques when applied for segmenting brain tumours accurately, according to experimental findings. In future the algorithm CAS- FCM can be used for tumor classification system.

REFERENCES

[1] S. K. H. Seere and K. Karibasappa, "Threshold Segmentation and Watershed Segmentation Algorithm for Brain Tumor Detection using Support Vector Machine," *European Journal of Engineering Research and Science*, vol. 5, no. 4, pp. 516–519, Apr. 2020.

[2] S. Chen, J. Wang, M. Zhang, M. Xu, W. Sheng at al., "Predicting Colon Cancer Outcomes from Histology Images Using Convolutional Networks," *International Journal of Radiation Oncology,Biology,Physics*, vol. 105, no. 1, pp. E129, 2019.

[3] X. Zhao, Y. Wu, G. Song, Z. Li, Y. Zhang, and Y. Fan, "A deep learning model integrating FCNNs and CRFs for brain tumor segmentation," *Medical Image Analysis*, vol. 43, pp. 98–111, 2018.

[4] I. E. Kaya, A. Ç. Pehlivanlı, E. G. Sekizkardeş, and T. Ibrikci, "PCA based clustering for brain tumor segmentation of T1w MRI images," *Computer Methods and Programs in Biomedicine*, vol. 140, pp. 19–28, 2017.

[5] R. Thillaikkarasi and S. Saravanan, "An Enhancement of Deep Learning Algorithm for Brain Tumor Segmentation Using Kernel Based CNN with M-SVM," *Journal of Medical Systems*, vol. 43, no. 4, 2019.

[6] H. Zunair and A.B. Hamza, "Sharp U-Net: Depthwise convolutional network for biomedical image segmentation," *Computers in Biology and Medicine*, vol. 136, pp. 104699, 2021.

[7] G. Wang, M. A. Zuluaga, W. Li, R. Pratt, P. A. Patel, et al., "DeepIGeoS: A Deep Interactive Geodesic Framework for Medical Image Segmentation," *IEEE Transactions on Pattern Analysis and Machine Intelligence*, vol. 41, no. 7, pp. 1559–1572, 2019.

[8] H. M. Balaha and A. E.-S. Hassan, "A variate brain tumor segmentation, optimization, and recognition framework," *Artificial Intelligence Review*, 2022.

[9] A. Işın, C. Direkoğlu, and M. Şah, "Review of MRI-based Brain Tumor Image Segmentation Using Deep Learning Methods," *Procedia Computer Science*, vol. 102, pp. 317–324, 2016.

[10] M. Elmezain, A. Mahmoud, D. T. Mosa, and W. Said, "Brain Tumor Segmentation Using Deep Capsule Network and Latent-Dynamic Conditional Random Fields," *Journal of Imaging*, vol. 8, no. 7, p. 190, 2022.

[11] M. B. naceur, R. Saouli, M. Akil, and R. Kachouri, "Fully Automatic Brain Tumor Segmentation using End-To-End Incremental Deep Neural Networks in MRI images," *Computer Methods and Programs in Biomedicine*, vol. 166, pp. 39–49, Nov. 2018.

[12] X. Zhou, X. Li, K. Hu, Y. Zhang, Z. Chen, and X. Gao, "ERV-Net: An efficient 3D residual neural network for brain tumor segmentation," *Expert Systems with Applications*, vol. 170, p. 114566, 2021.

[13] L. Pei, S. Bakas, A. Vossough, S. M. S. Reza, C. Davatzikos, and K. M. Iftekharuddin, "Longitudinal brain tumor segmentation prediction in MRI using feature and label fusion," *Biomedical Signal Processing and Control*, vol. 55, p. 101648, 2020.

[14] H. Khan, P. M. Shah, M. A. Shah, S. ul Islam, and J. J. P. C. Rodrigues, "Cascading handcrafted features and Convolutional Neural Network for IoT-enabled brain tumor segmentation," *Computer Communications*, vol. 153, pp. 196–207, 2020.

[15] M. Khoshkhoo, A. Arzehgar, F. Davarinia, and M. M. Khalilzadeh, "Brain Tissue Mr Image Segmentation with Anisotropic Textural Features," *SSRN Electronic Journal*, 2022.

[16] A. A. Sehgal, Y. Li, B. Lal, N. N. Yadav, X. Xu, J. Xu, J. Laterra, and P. C. M. van Zijl, "CEST MRI of 3-O-methyl-D-glucose uptake and accumulation in brain tumors," *Magnetic Resonance in Medicine*, vol. 81, no. 3, pp. 1993–2000, Sep. 2018.

[17] M. V. Gopalachari, M. Kolla, R. K. Mishra, and Z. Tasneem, "Design and Implementation of Brain Tumor Segmentation and Detection Using a Novel Woelfel Filter and Morphological Segmentation," *Complexity*, vol. 2022, pp. 1–9, 2022.

[18] A. Naseer, T. Yasir, A. Azhar, T. Shakeel, and K. Zafar, "Computer-Aided Brain Tumor Diagnosis: Performance Evaluation of Deep Learner CNN Using Augmented Brain MRI," *International Journal of Biomedical Imaging*, vol. 2021, pp. 1–11, Jun. 2021.

[19] R. Dharavath and K. Shyamala, "MRI Image Based Relatable Pixel Extraction with Image Segmentation for Brain Tumor Cell Detection Using Deep Learning Model," *Asian Journal Of Convergence In Technology*, vol. 7, no. 3, pp. 31–37, 2021.

[20] E. A. Zanaty, "Determining the number of clusters for kernelized fuzzy C-means algorithms for automatic medical image segmentation," *Egyptian Informatics Journal*, vol. 13, no. 1, pp. 39–58, Mar. 2012.

[21] A. G. Oskouei, M. Hashemzadeh, B. Asheghi, and M. A. Balafar, "CGFFCM: Cluster-weight and Group-local Feature-weight learning in Fuzzy C-Means clustering algorithm for color image segmentation," *Applied Soft Computing*, vol. 113, p. 108005, Dec. 2021.

[22] M. Roayaei, "On the binarization of Grey Wolf optimizer: a novel binary optimizer algorithm," *Soft Computing*, vol. 25, no. 23, pp. 14715–14728, 2021.

[23] M. Mohammdian-khoshnoud, A. R. Soltanian, A. Dehghan, and M. Farhadian, "Optimization of fuzzy c-means (FCM) clustering in cytology image segmentation using the gray wolf algorithm," *BMC Molecular and Cell Biology*, vol. 23, no. 1, 2022.

[24] F. ŞİŞİK and E. SERT, "Brain tumor segmentation approach based on the extreme learning machine and significantly fast and robust fuzzy C-means clustering algorithms running on Raspberry Pi hardware," *Medical Hypotheses*, vol. 136, p. 109507, Mar. 2020.

[25] H. Meharkure, "Brain Tumor Detection and Segmentation by Fuzzy C–Means (FCM) Algorithm Using LabVIEW,"

[26] Y. Gao, Z. Li, C. Song, L. Li, M. Li et al., "Automatic rat brain image segmentation using triple cascaded convolutional neural networks in a clinical PET/MR," *Physics in Medicine & Biology*, vol. 66, no. 4, pp. 04NT01, 2021.

[27] C. J. J. Sheela and G. Suganthi, "Automatic Brain Tumor Segmentation from MRI using Greedy Snake Model and Fuzzy C-Means Optimization," *Journal of King Saud University - Computer and Information Sciences*, vol. 34, no. 3, pp. 557–566, 2022.

[28] C. J. J. Sheela and G. Suganthi, "Brain tumor segmentation with radius contraction and expansion based initial contour detection for active contour model," *Multimedia Tools and Applications*, vol. 79, no. 33–34, pp. 23793–23819, Jun. 2020.

[29] C. J. J. Sheela and G. Suganthi, "Accurate MRI brain tumor segmentation based on rotating triangular section with fuzzy C- means optimization," *Sādhanā*, vol. 46, no. 4, Oct. 2021